# Experimental Correlation between Mechanical Non-Linearity in LAOS Flow and Capillary Flow Instabilities for Linear and Branched Commercial Polyethylenes

Susana Filipe, Iakovos Vittorias, Manfred Wilhelm*

An experimental correlation between the non-linear behaviour of commercial polyethylene melts in LAOS flow, and the pressure fluctuations associated with melt flow instabilities developed in capillary rheometry are presented. Polyethylene melts with enhanced non-linear behaviour under LAOS conditions present larger pressure fluctuations during capillary extrusion, and consequently, larger surface distortions on the extrudate. The combination of both methods can be a tool to predict the development of melt flow instabilities in the extrusion process of polyethylene melts, and can elucidate their correlation with material structural properties ($\overline{M}_w$, MWD and topology).
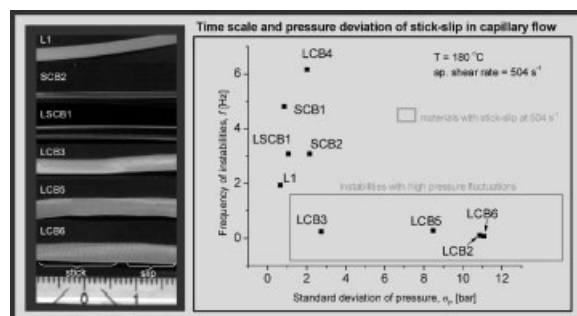
Introduction and Literature Review

Large interest has been focused on the study of slip phenomena of polymer melts, mostly due to its relevance in industrial processes[1–17]. This is particularly relevant, if one considers that the appearance of melt flow instabilities is a limitation for both maximum throughput and the type of material used in processes such as film and sheet extrusion.[18,19] Some authors suggest that the slip is mainly determined by the degree of adhesion, and thus by the level of interfacial interactions between the polymer and the wall interfaces.[18–20] However, other mechanisms have been introduced to explain the slip developed in polymer melts, one of the most relevant being the so-called coil-stretch transition.[18–20] According to the latter concept, the appearance of slip is attributed to a molecular mechanism, consisting of an entanglement/disentanglement process of the bulk polymer chains from the polymer film attached to the metal surface.[20] This phenomenon is more likely to occur when non-stationary boundary flow conditions are present at the die wall.[5] The critical shear stress σ_c, at which the transition from stationary to non-stationary boundary flow conditions occurs, was found to be independent of the temperature,[5] and to differ according to the viscoelastic properties of the material under investigation.

S. Filipe
Max-Planck-Institut für Polymerforschung, Postfach 3148, D-55021 Mainz, Germany
S. Filipe
Current address: Borealis Polyolefine GmbH, St. Peter Strasse 25, A-4021 Linz, Austria
I. Vittorias, M. Wilhelm
Max-Planck-Institut für Polymerforschung, Postfach 3148, D-55021 Mainz, Germany, and Institut für Technische Chemie und Polymerchemie, Universität Karlsruhe, Engesserstrasse 18, 76131 Karlsruhe, Germany
E-mail: wilhelm@polymer.uni-karlsruhe.de
I. Vittorias
Current Address: Basell, R&D Polymer Physics and Characterization, Industriepark Hoechst, D-65926 Frankfurt am Main, Germany

WILEY
InterScience®
DISCOVER SOMETHING GREAT

Moreover, and apart from of the mechanism used to explain the occurrence of melt flow instabilities, it is also recognised that the development of slip is highly dependent on the molecular structure and topology, as well as on the characteristics of the wall, e.g. geometry, construction material and roughness.[13,14]

Independently of the type of flow, either pressure driven (capillary) or drag flow (parallel plates), researchers agree with the importance of the extrapolation length b (ratio between the slip velocity v_s and the shear rate of the unbound layers near the wall $\dot{\gamma}_w$), as a determining factor on the type and magnitude of the melt flow instabilities developed. The kind of melt flow instability that develops, when a given shear stress is imposed on the material, is determined by the ratio between the extrapolation length b and the die diameter or gap between parallel plates, depending on whether a capillary flow or a drag flow is used.[20] Depending on the molecular weight and molecular architecture of the material, the extrapolation length might be significantly lower or reach values comparable to those of the die diameter or gap, as is the case of highly entangled polymers.[20] Therefore, when considering only the flow through a capillary die, materials with increasing molecular weights have a higher tendency to develop very abrupt instabilities, like for example, stick-slip.[20] Examples are high-density polyethylene (HDPE) or low-density polyethylene (LDPE) containing high-molecular weight tails. In contrast, when linear and short-chain branched (SCB) materials, with lower molecular weights and narrower molecular distributions are considered, the extrapolation length is considerably smaller, leading to the appearance of sharkskin.[20] The magnitude of the coil-stretch transition involved here is much lower.[20] This means that the slip will not develop at the bulk level, as occurs for long-chain branched (LCB), high-molecular weight and broad-molecular weight distribution materials, but rather on a molecular level with a time scale comparable to the characteristic relaxation time of the material. It is relevant to mention that both stick-slip and sharkskin are periodic defects characterised by a given frequency. Typically, the frequency of the developed instability is lower than 10 Hz for stick-slip and higher than 10 Hz for sharkskin. Furthermore, the deviations from the mean value of the pressure are usually several bars for the stick-slip instability and less than 0.1 bar for sharkskin.

The slip taking place in capillary flows, either in slit or circular dies was evaluated.[21,22] Moreover, similar attention was devoted to the evaluation and study of the slip developed in sliding plate rheometers.[23,24]

When considering flow through a capillary die, the presence of slip is usually manifested by the development of melt flow instabilities, namely sharkskin and stick-slip. In general, in what regards capillary flows, the available data is consistent with the hypothesis that slip is more frequent for highly entangled polymers, and less probable or absent for branched polymers or linear polymers with a low degree of entanglement.

The presence of slip during flow developed in parallel-plate rheometers has other consequences. One example is the continuous decay of the stress response during a large amplitude oscillatory shear (LAOS) measurement, which is in fact, the result of a change with time of the polymer-wall interfaces.[23] Previous research on slip developed in parallel-plate geometry, showed that the polymer properties (topology, molecular weight and molecular weight distribution) have an influence on the intensity at which the stress response decays, and on the strain amplitude upon which the onset of slip takes place.[23] Another manifestation of wall slip developed during flow in sliding plate rheometers is the appearance of complex non-periodic, asymmetric and in some situations even chaotic, stress responses.[25]

The development of slip in sliding plate rheometers is highly probable, when the materials are subjected to large amplitude deformations, as for example, LAOS flow. A significant number of publications have been devoted to the study of melt flow instabilities developed during LAOS flow. Examples are the evaluation of the slip arising from LAOS flow on monodisperse polystyrene melts,[26] concentrated solutions of high-molecular weight polystyrenes,[27] and PS solutions and melts.[28] In most cases, the above publications state that the appearance of different types of LAOS signals is attributed to the flow properties and to material constitutive instabilities.[26–28]

To the best of our knowledge, only a few publications have explored and analysed the slip phenomena being developed in both flow types (sliding plate and capillary flow)[22,23] for the same material. Particularly relevant in terms of capillary flows, is that slip is reduced or hindered by increasing the pressure, thus attenuating or suppressing extrudate distortions.[21] Independently of the type of flow, the onset of slip is related with the attainment of a given critical wall shear stress σ_c. The value of σ_c differs according to the flow, and depends on the molecular weight and molecular weight distribution.

In this article, we would like to address the correlation between the molecular weight, molecular weight distribution and topology and the appearance of melt flow instabilities in two types of flow, capillary and sliding plates.

The main purpose of this work is to evaluate the slip developed under capillary and during application of LAOS in parallel plates, for different commercial polyethylenes covering a broad range of molecular weights, molecular weight distributions, type and amount of branching. The polyethylene samples studied within the present work were characterised previously with respect to their topology (linear, SCB, LCB), molecular weight and molec-

ular weight distribution, via LAOS and Fourier-transform (FT) rheology, complemented with melt-state NMR and finite element LAOS simulations.[29] The non-linear behaviour of these melts, as quantified by the FT rheology parameters, e.g. $I_{3/1}(\gamma_0) = A(1 - 1/(1 - (B\gamma_0)^C))$ was found to depend on the polymer topology, molecular weight and polydispersity.

For the sliding plate geometry, the evaluation of slip was done via the analysis of the stress response developed during the application of LAOS. In capillary flows, the slip was evaluated by characterising the pressure profiles within the capillary die, associated with the development of melt flow instabilities. In both the cases, the raw data, i.e. the stress response for the LAOS flow and the pressure response for the capillary flow, were Fourier-analysed.

Experimental Part

Materials

A total of nine industrial polyethylene samples, supplied by TOTAL (Feluy, Belgium), were investigated. All samples were characterised with respect to their linear rheological properties, namely $G'(\omega)$, $G''(\omega)$ and $|\eta^*(\omega)|$.[29] Furthermore, the non-linear rheological behaviour in shear of these samples was quantified via FT rheology and correlated to their topology and polydispersity, combining the results of ^{13}C melt-state NMR and gel permeation chromatography (GPC) measurements.[29] The nomenclature used for the materials consists of the topology, the molecular weight $\overline{M}_w$, and the polydispersity index (PDI) ($\overline{M}_w/\overline{M}_n$), as shown in Table 1.

Dynamic Oscillatory Shear Measurements

Oscillatory shear measurements were undertaken on a TA Instruments ARES rheometer and an Alpha Technologies RPA2000 rheometer (Rubber Process Analyser). The ARES rheometer was equipped with a 1KFRTN1 torque transducer, detecting torques ranging from 4×10^{-7} to 0.1 Nm. A parallel-plate geometry with 13 mm diameter was used. This specific geometry allowed strains up to $\gamma_0 = 3$, while keeping the resulting torque within the transducer's limits. The RPA rheometer was equipped with a transducer whose operating range is from 10^{-4} to 5.6 Nm. In this apparatus, the sample was kept in a sealed test chamber, which was pressurised to about 6 MPa during the experiment. The measurement geometry used was a biconical die, with an opening half angle of 3°35′ and with large grooves to prevent slippage.[29]

LAOS and FT Rheology Measurements

The ARES and the RPA2000 rheometers were kept in a rigid and mechanically stable environment to reduce the mechanical noise level. The raw torque data was externally digitised using a 16-bit analogue-to-digital converter (ADC) card (model PCI-MIO-16XE, National Instruments, Austin, TX, USA) operating at sampling rates up to 100 kHz for one channel, or 50 kHz for two channels. The two channels allowed the measurement and averaging (oversampling) of the shear strain and torque 'on the fly'.[30,33]

All measurements were carried out after a periodic steady-state had been reached, with 20 cycles being recorded. The change of both the relative intensities and phases is negligible within more than 60 min of measurement (e.g. $I_{3/1} = 3 \pm 0.15\%$ and $\Phi_3 = 150 \pm 5°$). The measurements were repeated three times and were found to be reproducible with a typical deviation of less than 5% of the relative intensity, and 5° of the relative phase value (e.g. $I_{3/1} = 6 \pm 0.3\%$ and $\Phi_3 = 150 \pm 5°$). In order to compare the

Table 1. Investigated polyethylene samples: weight-average molecular weight $\overline{M}_w$, and polydispersity $\overline{M}_w/\overline{M}_n$ as determined by GPC. The total number of all branches (SCB and LCB) of four carbons and longer is identified and represents an upper limit of LCB.

Sample[a]	$\overline{M}_w$ kg·mol^{-1}	$\overline{M}_w/\overline{M}_n$	Comonomer	Estimated topology	LCB + SCB (>C4)/1000 CH$_2$[b]
L1	117	5.1	no	linear	0.0
SCB2	59	2.1	yes	SCB	4.5
SCB1	100	2.7	yes	SCB	2.1
LSCB1	71	2.3	octene	LCB and SCB	18.9
LCB4	145	8.6	yes	LCB-low SCB	0.8
LCB3	199	19.0	very low	LCB-low SCB	0.5
LCB6	206	18.0	yes	LCB-low SCB	0.9
LCB5	210	20.4	yes	LCB-low SCB	0.6
LCB2	234	15.6	very low	LCB	0.5

[a]The designations L, SCB, LSCB and LCB denote linear, short-chain branched, long and short-chain branched and long-chain branched, respectively; [b]Measured by melt-state ^{13}C NMR.

results from the ARES parallel-plate geometry with those from the RPA biconical die, a shift factor of 0.75 was applied.[34]

Capillary Flow Measurements

Optimised Set-up

Capillary flow measurements were carried out in a GÖTTFERT Rheo-tester 2000 capillary rheometer, fitted with a 9.5 mm diameter barrel and a slit die with 0.3 mm height, 3 mm width and 30 mm length (see Figure 1). In order to evaluate the critical shear rate, $\dot{\gamma}_c$, that determines the onset of melt flow instabilities, conventional flow curves were obtained by setting the temperature at 180 °C and varying the apparent shear rates from 5 to 4 000 s^{-1}.

The measurements described above were done specifically to analyse the pressure profiles associated with smooth surface, sharkskin and other melt flow instabilities. These measurements allowed the determination of a critical shear rate $\dot{\gamma} \cong 504$ s^{-1}, at which all the materials under study developed melt flow instabilities. These instabilities ranged from sharkskin to stick-slip, depending on the material properties. Additional measurements, in which the apparent shear rate was set constant (504 s^{-1}), were performed at 180 °C. The slit die used in this work is non-conventional, and was specifically designed in order to allow the evaluation of the pressure fluctuations at three different locations along its length ($L = 30$ mm), namely 3, 15 and 27 mm (these locations will be named along this work as tr1, tr2 and tr3, respectively). The 30 mm position refers to the die exit.[31] The evaluation of the pressure was done via fast acquisition pressure transducers (model 6812B, from KISTLER, Ostfildern, Germany). The electric shielding of the pressure transducers was optimised by means of a specific custom-built flexible copper mesh. With these protective measures, both the drift and the influence from external electric noise were minimised. The full details of the set-up will be published elsewhere.[32]
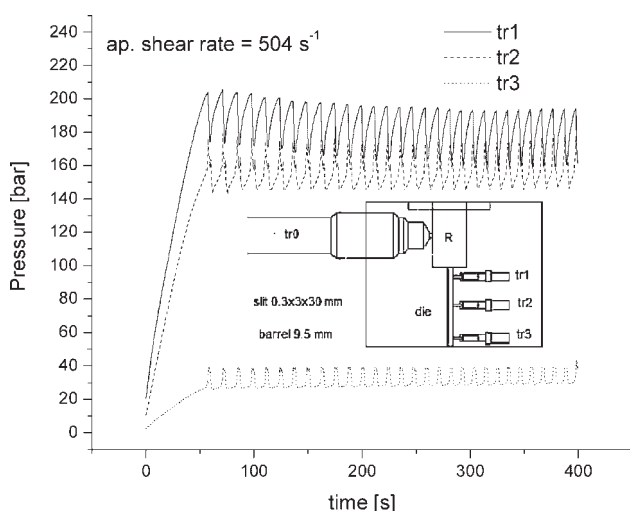

Figure 1. Example of recorded stick-slip pressure oscillations for stick-slip from the transducers in a slit die of $L = 30$ mm and a cross-section of 0.3 mm × 3 mm (see technical drawing). The results shown are for sample LCB2_234_15.6, at $\dot{\gamma}_{ap} = 504 \cdot$ s^{-1}.

The raw time data acquired with the piezoelectric pressure transducers, in the form of an electric potential, was converted to pressure data by means of three 5015A charge amplifiers from KISTLER. The raw pressure time data was then externally digitised resorting to a 16-bit ADC card, specifically a PCI-MIO-16XE ADC card, from National Instruments. The sampling rate used was 100 kHz, which resulted in a sampling rate of 33 kHz per channel. The raw pressure time data was collected and stored using a custom-written LabView^{TM} routine. The oversampling was performed using the method developed and outlined previously.[30,33,34]

The use of such fast response transducers, coupled with oversampling techniques,[29] allowed a substantial improvement by a factor of 1 000 and 100 in terms of both time and pressure resolution, respectively, when compared with conventional pressure transducers used in capillary rheometry.[31]

This is crucial for the determination of the pressure along the die length, evaluation and characterisation of sharkskin, which is known to be characterised by high frequencies and low-pressure fluctuations that are not detectable by the use of conventional pressure transducers. The evaluation of the pressure at the die itself is necessary to characterise melt flow instabilities such as sharkskin, which are known to have an origin at the die.

Analysis of Raw Data

The collected pressure data, which is optimised in terms of time and pressure resolution, was further treated using statistical (mean value, standard deviation, etc.) and Fourier analysis. After oversampling, Fourier analysis is performed on the pressure versus time data, as shown in Figure 2. When instabilities are absent, the spectra show a single peak located at $f = 0$ Hz, that reflects the mean value of the pressure (see Figure 2(a)). In the presence of melt flow instabilities, as for example sharkskin, stick-slip, or gross melt fracture, the Fourier spectra revealed peaks at frequencies $f = 0$ Hz and $f > 0$ Hz, as depicted in Figure 2(b). The additional peaks, located at higher frequencies, present a magnitude that matches with the standard deviation of the pressure, as shown in Figure 2(b). These peaks are located at a frequency that is the inverse of the related time scale of the instability.[31]

Results

Flow Instabilities in Capillary Flow

In order to be able to monitor all types of melt flow instabilities, i.e. those being developed along the die (sharkskin), and those having the reservoir as starting point (stick-slip), the pressure profiles were collected at position tr1. In conventional set-ups, it is only possible to measure the pressure at the reservoir. Thus, the pressure fluctuations associated with sharkskin cannot be monitored.

The type, magnitude and frequency of the different melt flow instabilities developed by the different materials during extrusion through a capillary die at a constant shear rate of 504 s^{-1} and temperature of 180 °C, are shown in Table 2 and Figure 3. The instabilities resulted in
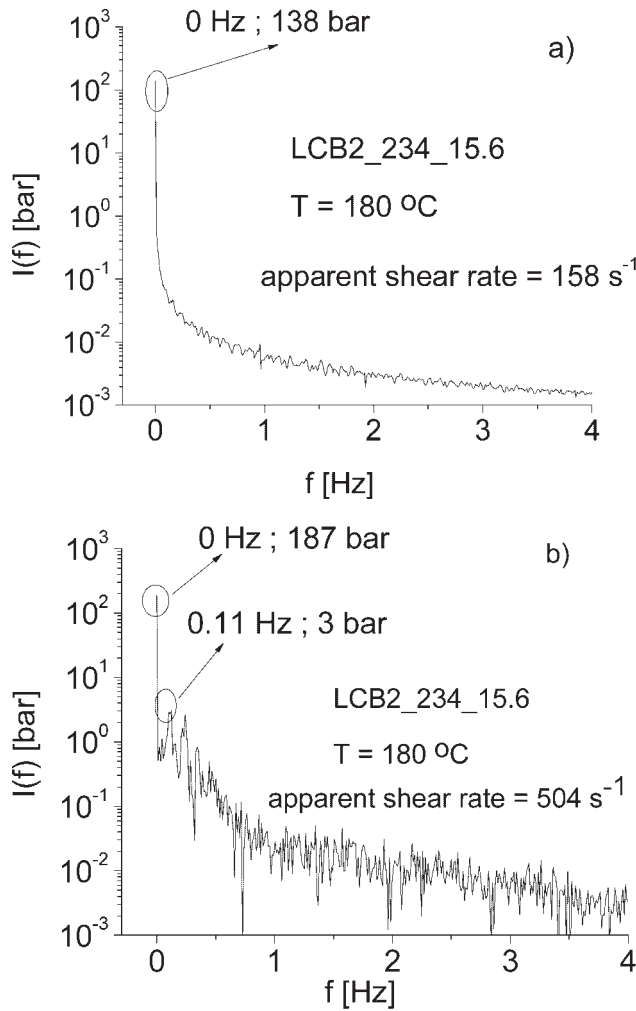
0 Hz ; 138 bar

a)

LCB2_234_15.6

T = 180 °C

apparent shear rate = 158 s^{-1}

0 Hz ; 187 bar

b)

0.11 Hz ; 3 bar

LCB2_234_15.6

T = 180 °C

apparent shear rate = 504 s^{-1}

Figure 2. Examples of Fourier spectra of the pressure data after oversampling: (a) data for $\dot{\gamma}_{ap} = 158$ s^{-1}, the surface of the extrudate was smooth and no peaks apart from the peak at $f = 0$ Hz are detected; (b) the pressure data corresponds to $\dot{\gamma}_{ap} = 504$ s^{-1}, the peak with the highest intensity is located at $f = 0$ Hz, corresponding to the mean pressure. The second peak, located at $f = 0.11$ Hz, gives the inverse of the time scale of the instability (specifically stick-slip) and its related pressure fluctuations. For both measurements, the material used was LCB2_234_15.6 and the data was recorded at position tr1, for $T = 180$ °C.

periodic fluctuations of the pressure, which are characterised by a given frequency and standard deviation.

Due to the industrial nature and inherent complexity of the samples under study, it is extremely difficult to separate the effects of molecular weight and polydispersity from those caused by the type and amount of branching. However, when analysing the frequency of the instabilities as a function of the standard deviation of the pressure, depicted in Figure 3, several observations are worth of remark. When considering only the molecular weight and polydispersity, and for these particular shear rate, temperature and die geometry, one can state that

Table 2. Critical strain amplitude $\gamma_{o,c}$ and maximum non-linear parameter A, as determined by LAOS at 180 °C for $\omega_1/2\pi = 0.1$ Hz. Standard deviation of the pressure, σ_P, measured at position tr1 of a slit die, for capillary measurements performed at a shear rate of 504 s^{-1} for $T = 180$ °C. The frequency of the melt flow instability was obtained from the Fourier analysis of the pressure signal at position tr1, for 180 °C and for an apparent shear rate of 504 s^{-1}.

Samples	$\gamma_{0,c}$	A	σ_P	f	Instability
		%	bar	Hz	
L1	1.00	7.0	0.65	1.93	sharkskin
SCB2	>3.00	1.0	2.15	3.08	sharkskin
SCB1	1.25	4.0	0.85	4.81	sharkskin
LSCB1	1.50	8.0	1.06	3.08	sharkskin
LCB4	0.75	10.0	2.02	6.16	sharkskin
LCB3	0.45	11.0	2.75	0.243	stick-slip
LCB6	0.50	11.0	11.08	0.075	stick-slip

materials with high-molecular weights and broad PDIs are more predisposed to develop stick-slip instabilities (LCB2, LCB3, LCB5, LCB6). Moreover, samples having lower $\overline{M}_w$ and PDI (SCB1, SCB2, LSCB1) presented sharkskin, which is an instability, characterised by considerably higher frequencies and lower pressure deviations, as compared to stick-slip (Table 2 and Figure 4). These results are in agreement with previous findings,[2,7,21] in which the detection and analysis of sharkskin was done using only morphological analysis, e.g. SEM. The results from this work provide an additional insight on the sharkskin phenomena, since the analysis of the melt flow instability is extended to the evaluation of the pressure at the die. Additionally, apart from LCB4, all the LCB materials
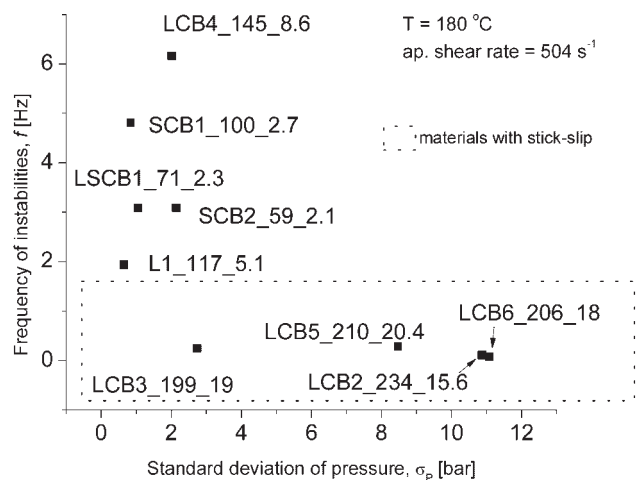

Figure 3. Frequency of the instability in capillary rheology at $T = 180$ °C and $\dot{\gamma}_{ap} = 504$ s^{-1} (as determined by Fourier analysis), $\dot{\gamma}_{ap}$ as a function of the standard deviation of the pressure.
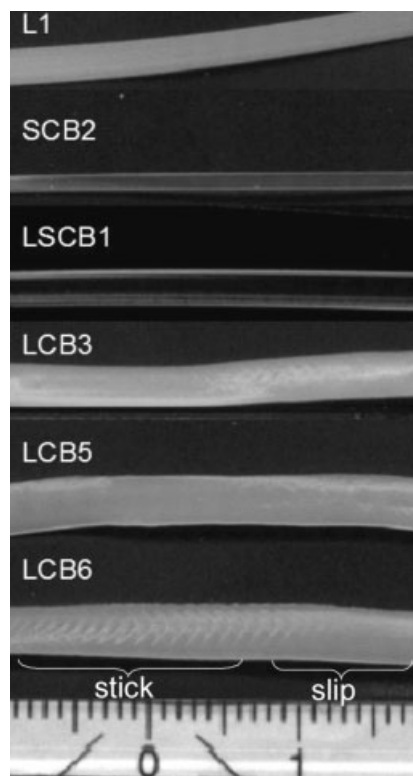
Figure 4. Capillary extrudates at 180 °C and for an apparent shear rate of 504 s^{-1}. L1, SCB2 and LSCB1 show a smooth surface, whereas LCB3, LC5 and LCB6 exhibit a stick-slip instability.

presented stick-slip instability for these specific conditions. The reason for this behaviour is related with the fact that LCB4 has the lowest molecular weight and polydispersity. Such properties delay the appearance of the stick-slip instability to a higher critical shear rate $\dot{\gamma}_c$. This was indeed observed for LCB4. The onset of stick-slip for LCB4 occurred at a higher critical shear rate, $\dot{\gamma}_c = 788$ s^{-1}.

Finally, it should be mentioned that stick-slip was not detected for the samples SCB1, SCB2 and LSCB1, at any of the applied shear rates used in this study, which ranged from 50 to 4 000 s^{-1}. With these observations, one might argue that for this particular set of samples, the absence of LCB together with low-molecular weights helps to release the stick-slip instability and improves the stability of the melt, when flowing through a capillary die.

In view of the above findings, one can understand the absence of sharkskin effect in LCB materials as an outcome of the improved melt strength of these samples, when comparing with SCB and linear ones. This is understandable if one regards the sharkskin instability as a defect due to the failure (or rupture) of the extrudate surface, while being subjected to an abrupt acceleration and high elongational stress at the die. On the other hand, one should also keep in mind that LCB and high-molecular weight materials have a higher tendency to develop

increased instabilities and complex vortices at the reservoir. This facilitates the appearance of more abrupt instabilities, e.g. stick-slip, helicoidal defect.

Investigation of LAOS Flow Via FT Rheology

As previously mentioned, FT Rheology was used to study different PE industrial samples with respect to their behaviour under the LAOS flow. This technique is described in more detail elsewhere.[34] The resulting non-linearities showed a dependency on both the molecular weight and topology.[29] For strain amplitudes above a critical value $\gamma_{0,c}$, the stress time signal exhibited an amplitude decay that indicates slip, as shown in Figure 5 and in qualitative agreement with Chen et al.[28] and Hatzikiriakos and Dealy.[22] As an example, the relative intensities of the second and third harmonic for LCB2, as measured with the ARES and the RPA2000, are depicted in Figure 6. The even harmonics and especially $I_{2/1}$ appeared at large strain amplitudes in the ARES, with their intensity being well above the noise level (typically $\approx 0.2\%$). The second harmonic becomes significant (above noise level) at the onset of the stress amplitude decay and it is found to be a useful indicator of secondary flows or generally instabilities.

The ARES and RPA2000 rheometers are different with respect to their tendency for slippage to occur. In the ARES, a flat open-rim geometry is used that will allow a higher level of surface slip. In contrast, the geometry of the RPA2000 consists of a closed cavity between dies with grooved surfaces, which suppresses slippage.[29] Furthermore, the high pressure of the chamber in case of the RPA2000 may be responsible for the absence of instabilities,
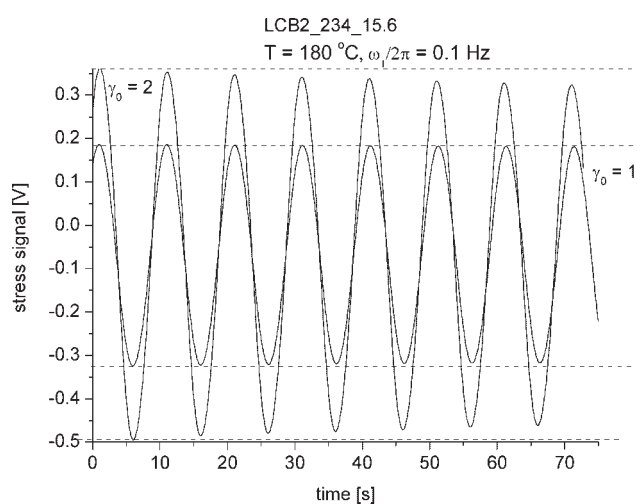

Figure 5. LAOS stress signals for a branched polyethylene, with strain amplitudes $\gamma_0 = 1$ and $\gamma_0 = 2$. The decay of the stress signal's amplitude can be observed in both cases and is attributed to slip.
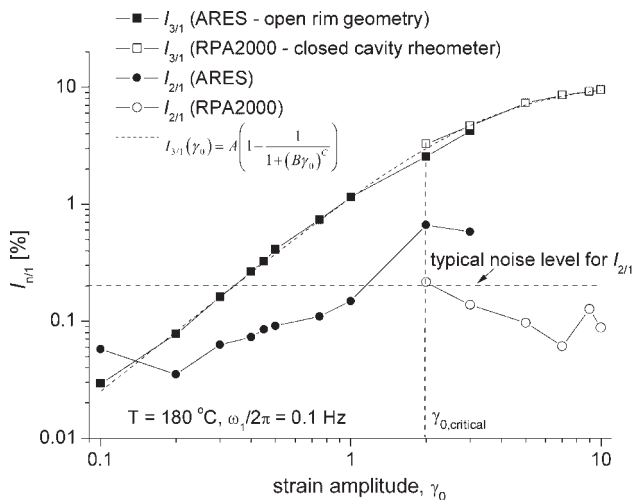
Figure 6. Relative intensities of the second and third harmonic as a function of strain amplitude, γ_o for LCB2_234_15.6. For measurements in the ARES rheometer, an open-rim geometry with smooth steel plates is used. For the case of the RPA2000, the sample is measured under pressure in a closed cavity between conical dies with grooved surfaces, thus surface slippage is suppressed.

Figure 7. Critical strain amplitude, $\gamma_{o,c}$, for the stress signal's amplitude decay as a function of the number of entanglements per chain, for LAOS at $T = 180\,°C$ with $\omega_1/2\pi = 0.1$ Hz. Open symbols correspond to linear and SCB samples. The line has a scaling exponent of -2 and is a guide to the eyes. The error in determining $\gamma_{o,c}$ is typically of the size of the data points.

especially those originating at the polymer/metal interface.[21] The stress time signals recorded during LAOS flow are highly non-linear. Nevertheless, their relative amplitude is generally constant and their periodicity is not distorted. Therefore, $I_{3/1}$, as measured in the RPA2000, corresponds mainly to the inherent constitutive material non-linearity, while in the ARES for $\gamma > \gamma_{0,c}$ the non-linear behaviour is considered as the result from both material non-linearity and additionally, surface flow instabilities.

As already stated, the critical $\gamma_{0,c}$ depends strongly on the material non-linearity and structure (e.g. $\overline{M}_w$ and PDI) and topology (e.g. SCB and LCB). The branching content and its type were found to influence the onset and evolution of the flow instabilities. Plotting $\gamma_{0,c}$ versus the average number of entanglements (Figure 7), it is obvious that no simple relation can be extracted between slip onset and the molecular weight, due to the influence of the polydispersities and the significant difference in branching between the investigated samples. Nevertheless, it is clear that the critical deformation for slip decreases with increasing molecular weight (see Table 2).

The critical strain amplitude for slip onset in LAOS is clearly reduced by the presence of LCB, as shown in Table 2. The presence of LCB increases the number of topological constraints for a polymer chain. Consequently, branching affects the onset of slip for a melt and its development: the latter is either related to elasticity and constitutive material properties, or to an entanglement/disentanglement process of bulk chains with adsorbed chains on the wall. For the case of the linear polyethylenes, the effect of a broad polydispersity is clearly observed. Large macro-
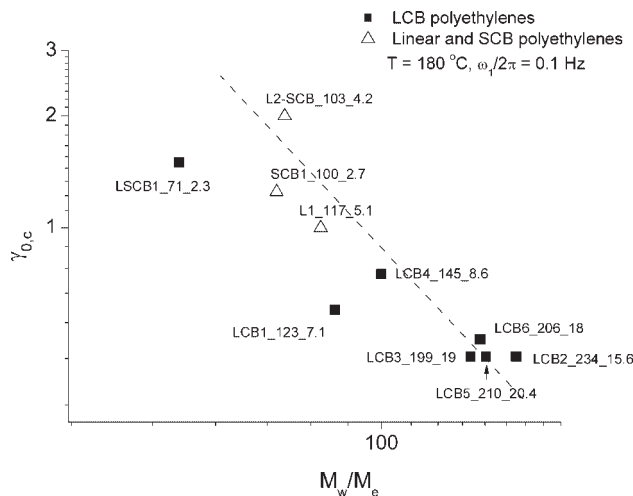
molecules induce instabilities at relatively low deformations and dominate the non-linear rheological behaviour.

We would like to address, as well, what is the possible origin of the slip found under LAOS flow. Due to the fact that the experimental conditions (type of surface, type of material and geometry, temperature, mechanical and thermal history) were kept constant, it is believed that the difference for the onset of slip in LAOS, determined via the decay of the stress signal with time, arises from molecular and structural differences ($\overline{M}_w$, MWD and branching). Such observations suggest that we deal with a constitutive instability which can be enhanced easily by flow type factors, e.g. surface type.

Discussion

The critical deformation and the flow conditions for the onset of slip are non-linear shear flow properties which are highly dependent on the molecular structure and topology. The development of slip has a constitutive nature, arising from the material properties, but is also related with the type of flow and geometry. A few questions on this topic still need to be addressed: when extremely large deformations are applied to a material, what is the predominant factor that controls the development of slip? Is it the material properties, e.g. $\overline{M}_w$, PDI, topology or the type of flow involved? Is it possible to predict the behaviour of a given material in terms of slip and other instabilities in a given type of flow, when the behaviour of this material in another type of flow is known?

Both the melt flow instabilities in capillary flows and the instabilities in LAOS, arise from the presence of slip, which in turn is related with the molecular properties and architecture. Consequently, an attempt was made to experimentally correlate these two types of instabilities. This was done by plotting the maximum non-linearity A as a function of the maximum standard deviation of the pressure σ_p, measured at the capillary die (Figure 8). It is important to keep in mind that A is a parameter derived from the non-linear behaviour as quantified via $I_{3/1}(\gamma_0)$, which combines non-linear viscoelasticity and flow characteristics.

The polyethylenes showing the highest non-linear character A, and the lowest critical strain deformation for the onset of slip $\gamma_{0,c}$ in a LAOS flow (LCB2, LCB3, LCB5, LCB6), exhibited the most dramatic melt flow instabilities, during extrusion through a capillary die, at a constant shear rate and temperature, as seen in Table 2 and Figure 8). This means that, independent of the type of flow, the materials with a higher level of LCB were those exhibiting a higher non-linear mechanical response, and also the ones which were more likely to flow in an unstable manner.

It is relevant to mention that the maximum non-linear character is determined, from the measurements carried out in the RPA2000 rheometer, for which, as explained before, surface slip is considered to be suppressed or even absent. Therefore, it can be stated that, a material with a higher non-linearity A, will have a higher tendency to develop slip, which has to do with both material topology and properties and type of flow. Furthermore, the onset
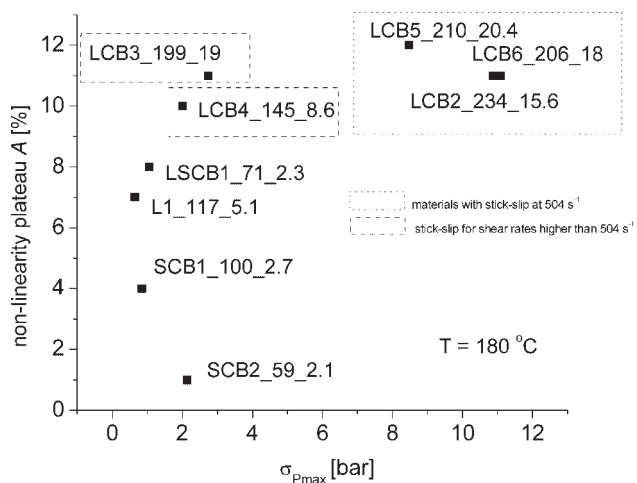
shear rates $\dot{\gamma}$, and strain amplitudes $\gamma_{0,c}$, for the occurrence of slip in capillary and LAOS flow, respectively, possess a similar dependency with respect to the material structural properties.

Conclusion

In this work, the non-linear rheological behaviour of industrial polyethylene melts and the flow instabilities occurring during extrusion were investigated. This was performed by correlating results from two non-linear rheological methods. The first method consists of an analysis of the pressure profiles along the die length in a conventional capillary rheometer.[31] The data obtained with this optimised set-up, is improved in terms of both pressure and time resolution and is later subjected to statistical and Fourier analysis. The second method consists of the application of FT rheology for LAOS flow experiments in a parallel-plate geometry and in a closed biconical shear cell.[29]

Both types of measurements apply non-linear shear deformation, although with different shear rates and time dependency of the shear rate. Independently of the flow field, the slip and general flow instabilities occur, being either a constitutive material instability and/or loss of adhesion or entanglement/disentanglement of the polymer chains.[35] The onset of melt flow instabilities can be detected in capillary rheometry via the critical shear rate $\dot{\gamma}_c$, determined by a change of slope in the apparent shear rate versus apparent shear stress curve. Under oscillatory shear conditions, the onset of slip can be identified by the critical strain $\gamma_{0,c}$, which is the strain at which the amplitude of the stress signal begins to decay. When subjected to high levels of shear stress, the analysed polyethylenes overcome both $\dot{\gamma}_c$ and $\gamma_{0,c}$, in capillary and in oscillatory shear flow, respectively. In both kinds of flow, the transition, established by $\dot{\gamma} > \dot{\gamma}_c$, and by $\gamma_0 > \gamma_{0,c}$, possesses a similar dependency with respect to the material structural properties.

The quantification of melt flow instabilities in capillary flow can be done via the advanced detection, with improved time and pressure resolution and further analysis of the time-dependent pressure. Deviations from the mean value of the pressure ($\Delta P \cong 5$–15 bar) and pressure fluctuations characterised by low frequencies (in the order of 0.01–0.5 Hz) are associated with stick-slip instability. Furthermore, in LAOS flow, the highest deviation from the linear behaviour is quantified via parameter A, determined from $I_{3/1}$ versus γ_0.

Polyethylenes that tend to slip at lower strain amplitudes $\gamma_{0,c}$ during LAOS, have also a higher non-linearity plateau A. Both properties were found to increase for samples that showed an increased pressure deviation, as

Figure 8. Maximum non-linear character as a function of the maximum pressure deviation ($T = 180\,°C$). The parameter A was obtained from LAOS measurements performed at 180 °C for a frequency of 0.1 Hz. The standard deviation of the pressure was determined for the pressure measured at position tr1 of a slit die, during capillary rheometry measurements performed at 180 °C for an apparent shear rate of 504 s^{-1}.

well as a lower critical apparent shear rate $\dot{\gamma}_c$ during capillary extrusion. In both cases, high molecular weight $\overline{M}_w$ and broad polydispersities induce the occurrence of non-linear phenomena during the flow at an earlier stage, i.e. for lower $\gamma_{0,c}$ and for lower $\dot{\gamma}_c$. Finally, the presence of short-chain branching suppresses the slip phenomenon in LAOS and the observed stick-slip distortions in extrusion. On the other hand, an increased LCB content leads to larger non-linearities in LAOS (as quantified via the FT rheology parameter A) and large pressure deviations in the capillary die, due to flow instabilities such as stick-slip.

[1] J. Doelder, R. Koopmans, *J. Rheol.* **2005**, *49*, 113.
[2] L. Robert, Y. Demay, B. Vergnes, *Rheol. Acta* **2004**, *43*, 89.
[3] H. Münstedt, M. Schmidt, E. Wassner, *J. Rheol.* **2000**, *44*, 413.
[4] F. Brochard, P. G. De Gennes, *Langmuir* **1992**, *8*, 3033.
[5] D. M. Kalyon, H. Gevgilili, *J. Rheol.* **2003**, *47*, 683.
[6] A. V. Ramamurthy, *J. Rheol.* **1986**, *30*, 337.
[7] E. S. Carreras, *Rheol. Acta* **2006**, *45*, 209.
[8] E. Miller, J. P. Rothstein, *Rheol. Acta* **2004**, *44*, 160.
[9] D. A. Hill, M. M. Denn, M. Q. Salmeron, *Chem. Eng. Sci.* **1994**, *49*, 655.
[10] J. W. H. Kolnaar, A. Keller, *J. Non-Newt. Fluid Mech.* **1997**, *69*, 71.
[11] A. Santamaría, M. Fernández, E. Sanz, P. Lafuente, A. Muñoz-Escalona, *Polymer* **2000**, *44*, 2473.
[12] M. Aguilar, J. F. Vega, A. Muñoz-Escalona, J. Martínez-Salazar, *J. Mater. Sci.* **2002**, *37*, 3415.
[13] S.-Q. Wang, *J. Rheol.* **1996**, *40*, 875.
[14] M. Fernández, J. F. Vega, A. Santamaría, A. Muñoz-Escalona, P. Lafuente, *Macromol. Rapid Commun.* **2000**, *21*, 973.
[15] C. Deeprasertkul, C. Rosenblatt, S.-Q. Wang, *Macromol. Chem. Phys.* **1998**, *199*, 2113.
[16] A. Allal, A. Lavernhe, B. Vergnes, G. Marin, *J. Non-Newt. Fluid Mech.* **2006**, *134*, 127.
[17] S.-Q. Wang, P. A. Drda, *Macromolecules* **1996**, *29*, 4115.
[18] M. M. Denn, *Annu. Rev. Fluid Mech.* **2001**, *33*, 265.
[19] R. G. Larson, *Rheol. Acta* **1992**, *31*, 213.
[20] S.-Q. Wang, *Adv. Polym. Sci.* **1999**, *138*, 228.
[21] S. G. Hatzikiriakos, J. M. Dealy, *J. Rheol.* **1992**, *36*, 703.
[22] S. G. Hatzikiriakos, J. M. Dealy, *J. Rheol.* **1992**, *36*, 845.
[23] S. G. Hatzikiriakos, J. M. Dealy, *J. Rheol.* **1991**, *35*, 497.
[24] H. M. Laun, *Rheol. Acta* **1982**, *21*, 464.
[25] M. D. Graham, *J. Rheol.* **1995**, *39*, 697.
[26] D. J. Henson, M. E. Mackay, *J. Rheol.* **1995**, *39*, 359.
[27] M. J. Reimers, J. M. Dealy, *J. Rheol.* **1998**, *42*, 527.
[28] Y. L. Chen, R. G. Larson, S. S. Patel, *Rheol. Acta* **1994**, *33*, 243.
[29] I. Vittorias, M. Parkinson, K. Klimke, B. Debbaut, M. Wilhelm, *Rheol. Acta* **2006**, *46*, 321.
[30] L. Hilliou, D. Van Dusschoten, M. Wilhelm, H. Burhin, E. R. Rodger, *Rubber Chem. Technol.* **2004**, *77*, 192.
[31] S. Filipe, A. Becker, M. Wilhelm, in: *Proceedings of the 3rd Annual European Rheology Conference*, Hersonissos, Crete 2006, p. 256.
[32] S. Filipe, A. Becker, M. Wilhelm, to be published.
[33] D. Van Dusschoten, M. Wilhelm, *Rheol. Acta* **2001**, *40*, 395.
[34] M. Wilhelm, *Macromol. Mat. Eng.* **2002**, *287*, 83.
[35] A. S. Yoshimura, R. K. Prud'homme, *Rheol. Acta* **1987**, *26*, 428.